Altered Upper Airway and Soft Tissue Structures in the New Zealand Obese Mouse

Michael J. Brennick[1], Allan I. Pack[1,2], Kei Ko[1], Eugene Kim[1], Stephen Pickup[3], Greg Maislin[1,2], and Richard J. Schwab[1,2]

[1]Center for Sleep and Respiratory Neurobiology; [2]Division of Sleep Medicine, Department of Medicine, University of Pennsylvania School of Medicine, Philadelphia, Pennsylvania; and [3]Department of Radiology, Hospital of the University of Pennsylvania, Philadelphia, Pennsylvania

***Rationale*: The effect of obesity on upper airway soft tissue structure and size was examined in the New Zealand Obese (NZO) mouse and in a control lean mouse, the New Zealand White (NZW).**

***Objectives*: We hypothesized that the NZO mouse has increased volume of neck fat and upper airway soft tissues and decreased pharyngeal airway caliber.**

***Methods*: Pharyngeal airway size, volume of the upper airway soft tissue structures, and distribution of fat in the neck and body were measured using magnetic resonance imaging (MRI). Dynamic MRI was used to examine the differences in upper airway caliber between inspiration and expiration in NZO versus NZW mice.**

***Measurements and Main Results*: The data support the hypothesis that, in obese NZO versus lean NZW mice, airway caliber was significantly smaller ($P < 0.03$), with greater parapharyngeal fat pad volumes ($P < 0.0001$) and a greater volume of other upper airway soft tissue structures (tongue, $P = 0.003$; lateral pharyngeal walls, $P = 0.01$; soft palate, $P = 0.02$). Dynamic MRI showed that the airway of the obese NZO mouse dilated during inspiration, whereas in the lean NZW mouse, the upper airway was reduced in size during inspiration.**

***Conclusions*: In addition to the increased volume of pharyngeal soft tissue structures, direct fat deposits within the tongue may contribute to airway compromise in obesity. Pharyngeal airway dilation during inspiration in NZO mice compared with narrowing in NZW mice suggests that airway compromise in obese mice may lead to muscle activation to defend upper airway patency during inspiration.**

Keywords: obstructive sleep apnea; magnetic resonance imaging; body fat distribution; tongue; upper airway

Obesity is the most prevalent risk factor for obstructive sleep apnea (OSA) (1–3). Obese patients with OSA have a narrowed upper airway even during wakefulness, as demonstrated by multiple imaging modalities (4–8). However, the mechanisms by which obesity leads to a narrowed upper airway and OSA are unknown. This effect of obesity is found not only in humans but has also been observed in several animal models of obesity. Airway narrowing and increased collapsibility have been shown in the obese Zucker rats (9–12), and increased upper airway resistance has been demonstrated in obese pigs (13, 14).

However, there have been no studies of the effects of obesity on the upper airway in mouse models. Mouse models have been critical for the identification of genes conferring risk for obesity (15, 16) and cardiovascular disease (17). Thus, the mouse has become a key model for biomedical research (18). Of the currently available obese mouse models, the New Zealand Obese (NZO) mouse, a polygenic mutant on a New Zealand (NZ) background (19), is an excellent potential model for the study of obesity and whether obesity affects the size of upper airway structure. Lean New Zealand White (NZW) mice can serve as age-matched lean controls for the obese NZO mice. Obesity in the NZO mouse is polygenic (20) and the NZO has features of the metabolic syndrome (i.e., insulin resistance, diabetes [21], hypercholesterolemia, hypertension [22], and resistance to leptin [23]).

We hypothesized that the obese NZO mouse has upper airway narrowing, as described in other obese animal models (9, 12, 14, 24). Support for this hypothesis comes from the unusual observation by staff at the Jackson Laboratory (Bar Harbor, Maine) that obese NZO mice occasionally sleep upright (*see* Figure E1 in the online supplement). This sleeping posture may be an adaptation to upper airway compromise in these mice.

The study of obese NZO mice, when compared with the lean NZW controls, allows for the evaluation of airway size and whether obesity affects other upper airway structures and function. We anticipated that the volume of the parapharyngeal fat pads would be greater in NZO mice than in leaner NZW mice, as was previously shown in obese human patients with OSA (6, 7, 25). It has also been shown that obese humans have fat infiltration of their tongue, which increases with the degree of obesity (26). This likely contributes to enlargement of the tongue, and we have shown that increased tongue size in patients with OSA is a risk factor for OSA (6, 27). Fat has also been described as infiltrating the soft palate in obese humans (28, 29). Moreover, increased volume of the lateral pharyngeal walls has also been described in patients with OSA when compared with matched controls (7, 30); although the role of fat in this enlargement is unknown. Thus, in addition to measuring the dimensions of the upper airway, we examined the size of key upper airway structures among obese NZO and lean NZW mice, specifically the volume of the parapharyngeal fat pads, tongue, soft palate, and lateral pharyngeal walls. We hypothesized that these structures would be larger in

AT A GLANCE COMMENTARY

Scientific Knowledge on the Subject

Obesity results in upper airway compromise, and the mechanism explaining this relationship remains unclear.

What This Study Adds to the Field

In addition to the increased volume of pharyngeal soft tissue structures, direct fat deposits within the tongue may contribute to airway compromise in obesity. Airway compromise in obese mice may lead to muscle activation to defend upper airway patency during inspiration.

(*Received in original form September 11, 2008; accepted in final form November 6, 2008*)

Supported by National Institutes of Health grants HL-60287, HL-66611, HL-67948, HL-072067, EB-01780 and HL-077838 (Section 8.28 Upper Airway: Sleep).

Correspondence and requests for reprints should be addressed to Michael J. Brennick, Ph.D., Center for Sleep and Respiratory Neurobiology, 3624 Market Street, Suite 205, Philadelphia, PA 19104. E-mail: brennick@mail.med.upenn.edu

This article has an online supplement, which is accessible from this issue's table of contents at www.atsjournals.org

Am J Respir Crit Care Med Vol 179. pp 158–169, 2009
Originally Published in Press as DOI: 10.1164/rccm.200809-1435OC on November 7, 2008
Internet address: www.atsjournals.org

obese NZO mice than in leaner NZW mice. To ensure that any differences observed were not simply the result of altered craniofacial anatomy, we also examined the size of the mandible between the two mouse genotypes.

If the upper airway soft tissue structures were enlarged in the NZO mice, as hypothesized, we anticipated that this would lead to a narrowing and an alteration in other aspects of the function of the upper airway. In a model previously studied, the English bulldog (24, 31), we observed that the upper airway was actively dialated during inspiration to overcome the effect of the enlarged surrounding soft tissues. In English bulldogs, the upper airway area during inspiration was greater than expiration, reflecting this active dilatation. In contrast, the upper airway in normal dogs is passive and hence has a greater area during expiration, due to positive intraluminal pressure, than during inspiration (24). Thus, an additional comparison between obese NZO and lean NZW mice was to assess the dynamic changes in airway area during the respiratory cycle.

These hypotheses were all addressed by novel magnetic resonance imaging (MRI) techniques that we developed to study the upper airway in mice. Two different MRI strategies were used. The first used a three-point Dixon spin echo protocol (32) to study fat distribution and volume of the upper airway structures. The second used a gradient-recalled echo protocol to evaluate dynamic changes in the upper airway across the respiratory cycle. Some of the results of this study have been previously reported in abstract form (33).

METHODS

For an additional description of the METHODS *see* the online supplement. With the approval of the Institutional Animal Care and Use Committee of the University of Pennsylvania, MRI experiments were performed in two different protocols, a spin echo three-point Dixon protocol for anatomy and fat discrimination, and gradient-recalled echo protocol used to acquire a time series of images during breathing to assess cross-sectional area in the pharynx of the airway at discrete time-points during respiration. For the Dixon spin echo protocol, we studied 12 NZW and 8 NZO mice, and in the time series protocol there were 13 NZW and 11 NZO. Male mice were studied in every case.

Each mouse was positioned on a platform with a nose cone for anesthesia (1.0 to 2.0% isoflurane in oxygen) and adjacent to two sample tubes (0.5 × 10 cm) containing water and mineral oil, to provide reference signals for fat/water discrimination. The mice were placed supine in the coil in a custom cradle that provided a secure hood for breathing and support for the mouse body. We defined the angle of cervical spinal to the brain midline (parallel to the top of the skull) in the mid-sagittal images as the head to neck angle measured on the scout set-up images. A monitoring system (Small Animal Instruments, Stony Brook, NY) used a compliant pressure sensor positioned over the diaphragm to measure respiratory rate and to generate a trigger signal for gating the MRI to the respiratory cycle. In a respiratory-gated MRI-image matrix many single-data line scans are acquired at the same point in time in the respiratory cycle controlled by the trigger signal. Thus, respiratory-gated image acquisition prevents motion artifact (image blurring), because the image is captured at the same time (and position) in the respiratory cycle. The physiologic monitoring system also regulated core temperature at 37°C using a feedback-controlled warm-air source coupled with a rectal thermistor.

MRI Protocols

MRI was performed in a 4.7 Tesla magnet with an INOVA Console, (Varian, Palo Alto, CA) using a 65 mm ID Litz coil (Doty, Columbia, SC). A spin-echo 3-point Dixon protocol (32) produced two image series, one proton density and one fat density image series (Figure 1). In each Dixon protocol acquisition, two calibration tubes (one filled with mineral oil, one with water) were placed near the region of interest and were used to establish fat and water intensity levels for image analysis (Figure 1). The multislice Dixon study in the axial orientation was performed with respiratory gating (triggered to the expiratory phase) in spontaneously breathing mice with slice positions spanning the head and pharyngeal airway (matrix = 256 × 256; field of view [FOV] = 35 × 35 mm; slices = 18 contiguous; thickness = 1.0 mm; echo time [TE] = 8.6 ms; repetition time [TR] = respiratory rate or approximately 800 ms; averages = 4 [signal to noise is improved with the number of averages]). The protocol was repeated in the sagittal orientation (matrix = 256 × 256; FOV = 60 × 60 mm; slices = 5 near the midline only [scout images to orient the axial images]). At the conclusion of the head/neck study and while under anesthesia, mice were killed (intracardiac saturated KCl), and a whole-body Dixon study from the neck to the tail was performed (matrix = 256 × 256; FOV = 40 × 40 or 42 × 42 mm [depending on the girth of the abdomen]; thickness = 2.0 mm; TE = 8.6 ms; TR = 2.0 s; averages = 2). In two representative NZO and NZW mice, a 3D (overnight) spin-echo protocol (TE = 10 ms; TR = 300 ms; averages = 2; FOV = 40 × 40 × 80 mm; isotropic voxel size = 0.156 mm) was performed that spanned the head to abdominal region. This long imaging time provided excellent 3D spatial resolution. For these studies animals were killed (KCl intracardiac injection, under isoflurane anesthesia) prior to imaging.

The second MRI protocol (gradient-recalled echo) was used to acquire a time series of images using the respiratory gating method described above. For these images the MRI acquisitions were triggered at the onset of inspiration (Figure 2). However, given the slight system delay before the trigger was delivered to the MRI, the first image of the six-image sequence coincided with mid-onset (not early-onset) inspiration. Figure 2 shows the physiological monitor data and the respiratory pressure tracing with the timing of the gradient-recalled echo images indicated. The time series of six images (with 75 ms between images) in each breathing cycle (matrix = 128 × 128; FOV = 3.2 mm; slice thickness = 1.0 mm; TE = 3 ms; TR = 12 ms; averages = 4) were acquired in a multiple (3-slice) acquisition. Three additional acquisitions (each acquisition covered 3 mm) were obtained to cover a 12-mm volume of the pharynx.

Although each set of 12 contiguous axial slices were aligned (from the rostral to caudal pharynx) using the same methods for image analysis described below, the cross-sectional airway area was analyzed at only a single location in each mouse in the hypopharynx, as shown on the sagittal image in Figure 3 (*see* RESULTS and DISCUSSION). Because our goal was to compare inspiration and expiration, two of six time series at each slice location were chosen, one at mid-to-late inspiration ("inspiration") and the second (image number five of the six images) at the mid-expiratory phase ("expiration") of the breath.

All the mice were imaged in the supine position (none were imaged prone). We found in preliminary experiments that the viability of mice was reduced when they were studied in the prone position. We also used a pressure-sensitive "pillow-transducer" to monitor and record respiration. This method is noninvasive, easy to use, and provides a reliable trigger signal to initiate the respiratory-gated MRI. Although it would be possible, the use of this pressure-pillow method has not been developed for rodents in the prone position. We therefore used the supine position and made certain that the head-to-neck angle was constant throughout the experiments. We chose the supine position for physiological (viability) and technical reasons and used it in a consistent fashion.

We studied both live and postmortem mice (immediately following death). All the upper airway studies were performed in live, spontaneously breathing, anesthetized mice. Studies on the fat distribution in the chest and abdomen were performed in postmortem mice. Live studies of the upper airway allowed us to acquire images at both inspiration and expiration and while accounting for respiratory motion using the gated-imaging protocol. In the chest and abdomen, live imaging would have required cardiac and respiratory-combined gating that would have extended the overall MRI acquisitions time and without any significant contribution to the question of how fat was distributed in the mice. The 3-D volumetric MRI was acquired overnight in postmortem mice.

Image Analysis

MRI data were analyzed using Image J software (1.33u, NIH http://rsb.info.nih.gov/ij/) for airway size analysis, VIDA software (30) for soft-tissue segmenting and volume measurements, and Amira software (Mercury Computer Systems Inc., Chelmsford, MA) for 3D image

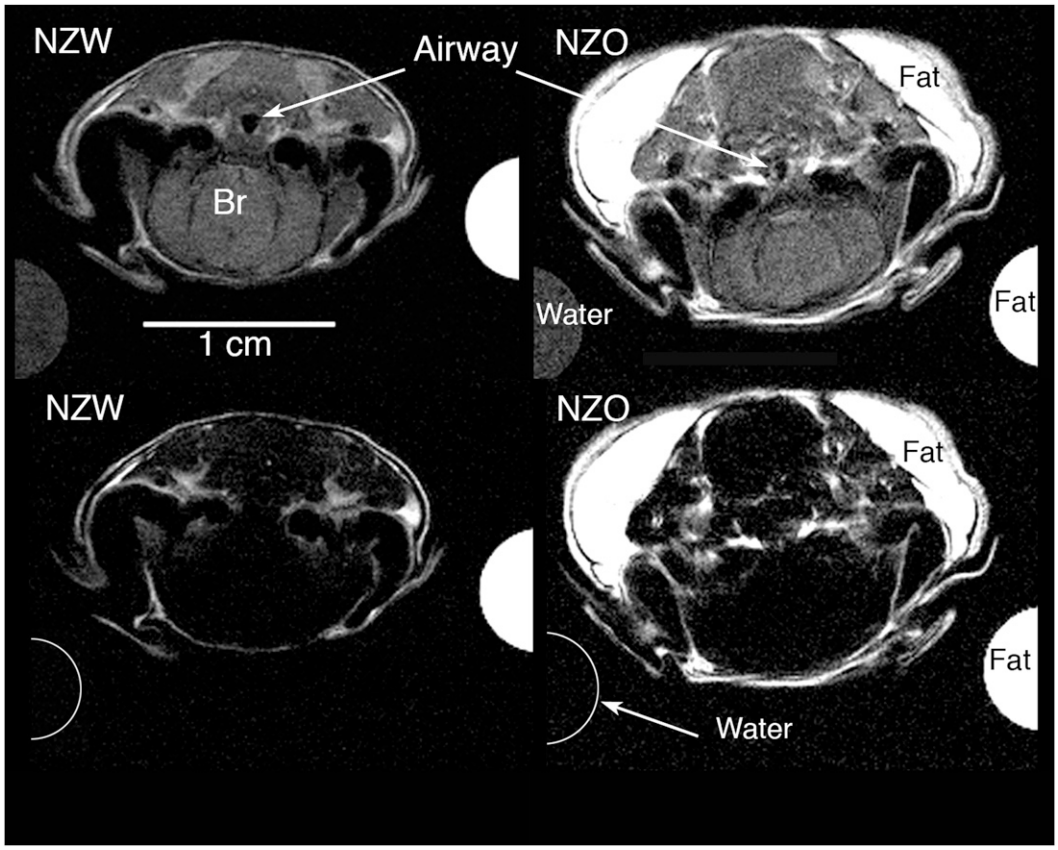

Figure 1. Four axial magnetic resonance images were obtained from the Dixon protocol at the level of the hypopharynx (caudal pharynx) in representative New Zealand White (NZW) and New Zealand Obese (NZO) mice. The *top row* shows proton-weighted images (for soft tissue contrast and segmentation) and the *bottom row* shows fat-weighted images (for fat segmentation and threshold analysis). The *half circles* on left and right of each image show the partial cross-section of the water and mineral oil (fat) phantoms. In the *top row* both the water and fat cross-sections can be seen at the resonant frequency for water. In the *bottom row,* only the fat oil phantom has a white intensity at the resonant frequency for fat; the water phantom shows the water signal intensity is completely suppressed. The use of water and oil phantoms provided calibration signals for the threshold analysis. The airway caliber in the *top row* (proton weighted images) is larger in the NZW mice compared with NZO mice, and there is more fat (in the fat-weighted images, *bottom row*) in the NZO mice compared with NZW mice. The upper airway is not well delineated in the fat-weighted images (*bottom row*) because the soft tissues, immediately adjacent to the airway, have little fat content.

renditions. Soft-tissue volumes were measured in the pharynx and included the tongue, soft palate, lateral pharyngeal walls, masseter muscles, and parapharyngeal fat deposits. Measures of the linear maximum mandibular width were also taken. (For definitions of these structures, *see* Figures E2 to E13 in the online supplement.) We assessed mandibular size to ensure that there was no difference in craniofacial dimension between the NZO and NZW. From the whole-body MRI protocol, four regions: the neck, thoracic, upper abdominal,

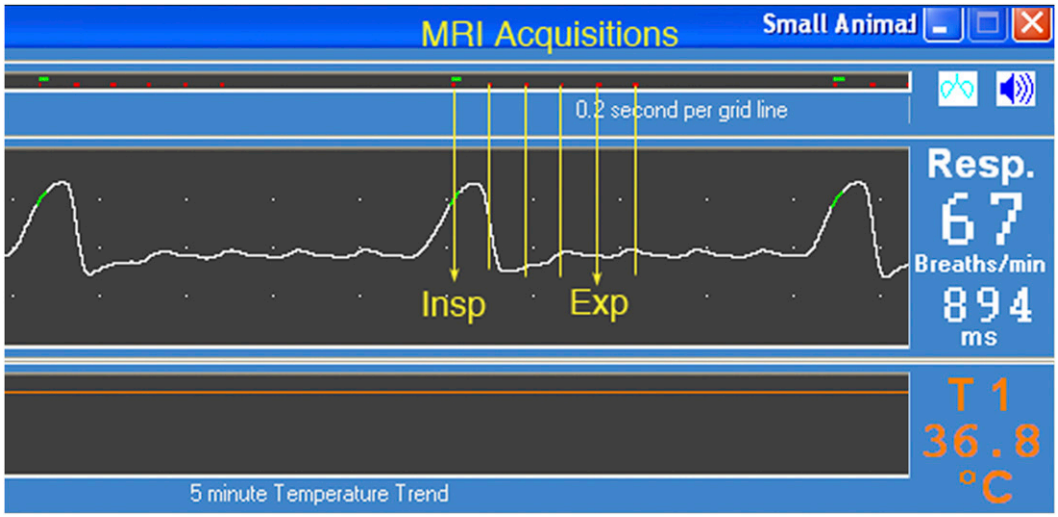

Figure 2. Physiological recordings during respiratory-gated cine magnetic resonance imaging (MRI) acquisitions. In this figure, the respiratory pressure trace (obtained from the pressure pillow on the mouse abdomen) is shown in the window above the temperature readout window. The respiratory trace shows the increased abdominal pressure (*upwards hump*) during each inspiratory effort followed by a relatively smooth period of no abdominal pressure change during expiration. The Small Animal Instruments, Inc. (Stony Brook, NY) software generates a trigger signal the same point during each inspiration (*green bar* shown on the respiratory signal) and that trigger initiates the MRI acquisition (*red dots*). The MRI multislice time-series protocol-acquired data from three axial slices at the six time-points (*red dots*) spaced 75 ms apart. We analyzed the six images and used only the first (Insp) and fifth (Exp) images to represent inspiration and expiration, respectively. The ''gated'' acquisition is repeated 128 times (once for each data line in the image matrix) with four averages to increase signal to noise for a total of 512 times, or 512 breaths, because each breath provided one line of data acquisition for the MRI protocol. Given a typical respiratory rate of 894 milliseconds per breath, the scanning time would be 457 seconds or approximately 7.5 minutes. Temperature (*lower window trace*) was monitored by rectal thermistor that was part of a feedback-controlled hot air–warming system to maintain mouse body temperature while under isoflurane anesthesia.

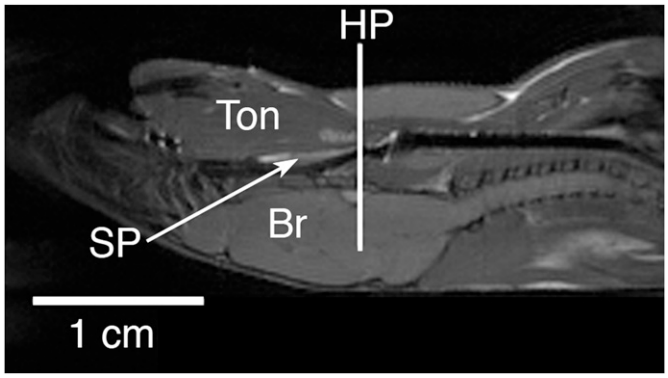

Figure 3. Mid-sagittal MRI of representative New Zealand White (NZW) mouse (in supine position) highlighting the location (hypopharyngeal [HP] region) where the transverse axial MRI of airway was obtained. The airway analysis was performed in the HP region. The image scale is noted (horizontal bar equals 1 cm). Ton = tongue; SP = soft palate; Br = brain.

and lower abdominal, were defined from anatomical landmarks. The neck region was defined as the first appearance of the tympanic bulla to the first appearance of the lungs (Figures E16 and E17); the thorax from the top of the lungs to the diaphragm (Figures E18 and E19); the upper abdomen from the diaphragm to the caudal margin of the kidneys (Figures E20 and E21); and the lower abdomen from the caudal margin of the kidneys to the beginning of the tail (Figures E22 and E23). In these four regions subcutaneous fat, visceral fat, and total tissue volume (i.e., all tissues bound within the skin) were quantified. On the Dixon images, fat was identified using a threshold subroutine (Image J) whereby the intensity of the calibrating mineral oil sample (Figure 1) in the fat-weighted images provided the minimum fat threshold level (white) and the water phantom (in the same fat-weighted image; Figure 1) was equivalent to the background noise (black).

Statistical Analysis

The primary objective of our study was to characterize differences between NZO and NZW mice in the volume of upper airway soft tissue structures and fat distribution. A total of 27 variables (*see* Table E1 for a list of the measurements categorized by domain; note that airway area was limited to "location 8") were chosen for analysis. The impact of multiple comparisons was addressed by assessing the false discovery rate (FDR) (34), a quantitative method that has been applied to control the effects of multiple comparisons in gene discovery (35) and in functional MRI evaluations (36). Simulation-based computations using the SAS procedure MULTTEST (SAS version 9.1, SAS Institute, Cary, NC) preserved the correlation structure among tests, maximizing statistical power and enabling the use of Student's *t* tests to assess the strength of the signals reflecting real differences in the variables. All 27 Student's *t* tests were performed using a nominal P value of 0.05 while computing the fraction of rejected null hypotheses expected to be falsely rejected (i.e., the false discovery rate). Nominal P values are reported, but variables not significant within the false discovery set are expressed as NS (not significant).

We used analysis of variance (with significance at $P < 0.05$) to analyze the results of the respiratory gated time sequenced study of airway sizes at a single airway locus, and we sought to answer the following questions: (*1*) is there an overall difference between the NZW and NZO for upper airway cross-sectional area in inspiration and in expiration, and (*2*) are there differences in the changes of airway dimensions between expiration and inspiration (i.e., expiratory cross-sectional area minus inspiratory cross-sectional area) between NZW and NZO mice?

RESULTS

Characteristics of Mice Studied

Two groups of mice were studied. In group 1 the size of the upper airway structures were evaluated, and in group 2 the dimensional changes in upper airway caliber during respiration were assessed. In both groups, NZO and NZW mice were matched for age and sex (male) and there were no significant differences in age ($P = 0.59$ and 0.12 for groups 1 and 2, respectively). As expected, the mean weight of NZO was substantially greater than the mean weight of NZW ($P < 0.0001$) for both groups (Table 1). Respiratory rate during the MRI studies was also compared between NZW and NZO mice and did not differ significantly in either group. The head-to-neck angle was measured in a representative selection of mice (n = 6 in NZW and n = 6 in NZO) from the scout set-up images. There was overall, no significant difference in head-to-neck angle between mice ($P = 0.13$; NZW = 145° ± 3.7°; NZO = 151°± 7.8°; mean ± SD) indicating that the head and neck position during the magnetic resonance scanning was similar between the two groups of mice.

Upper Airway Size–Dynamic Measurements

We compared upper airway cross-sectional areas in the hypopharyngeal region, just beyond the distal edge of the soft palate where the nasal and oropharyngeal airways are combined in a single lumen (Figures 1 and 3). When compared at the hypopharyngeal level, the cross-sectional area was similar in inspiration and not significantly different between NZW and NZO mice, but in expiration the airway was smaller in the NZO mice than in the NZW mice ($P < 0.03$) (Table 2). Further examination showed that the hypopharyngeal cross-section became smaller in the NZW mice from expiration to inspiration ($P < 0.006$), whereas in the NZO mice the opposite occurred, and the airway area was larger in inspiration than expiration ($P < 0.002$). Thus, a major difference between NZO and NZW mice was in the dimensional changes between expiration and inspiration. The NZO mice showed inspiratory dilation of the upper airway, whereas the NZW mice exhibited an increase in airway cross-sectional area during expiration (*see* movies in the online supplement). The calculated difference between the inspiratory cross-sectional area and that during expiration was significantly different ($P < 0.0002$; Table 2) in the NZO compared with the NZW mice (in the NZW mice this difference was positive but in the NZO mice it was negative).

Overall Analysis

Significant group differences were found for 22 of 27 measurements based on the criterion that the FDR must be less than 0.05 (observed FDR = 0.025). The complete list of variables and mean values for NZO and NZW mice are summarized in Tables E1 and E2. All of these 22 variables had nominal significance ($P < 0.021$). The expected number of false positives is 0.025 times 22 or 0.55 (i.e., <1). Thus, of the 22 significant NZO versus NZW differences, less than 1 are expected to be false positive. Because only 1 of 22 measurements is expected to

TABLE 1. EXPERIMENTAL DATA FOR MOUSE GROUPS

	N	Age, (*wk*)	Weight, (*g*)	Respiration Rate, (*breaths/min*)
Group 1: static analysis				
NZW	12	23.1 ± 5.8	35.7 ± 1.9**	73.0 ± 12.2
NZO	8	21.6 ± 5.9	54.1 ± 7.2**	69.1 ± 10.9
Group 2: respiratory timed series MRI				
NZW	13	23.1 ± 3.4	34.7 ± 1.3**	71.9 ± 9.5
NZO	10	21.0 ± 2.9	50.37 ± 4.0**	77.0 ± 13.8

Definition of abbreviations: MRI = magnetic resonance imaging; NZO = New Zealand Obese; NZW = New Zealand White.

Values are means ± SD. Within each group all values were not significantly different between NZW and NZO mice except **$P < 0.0001$.

TABLE 2. DYNAMIC IMAGING CROSS-SECTIONAL AREA MEASUREMENTS

	NZW	NZO	NZW vs. NZO
Insp cross-sectional area, mm^2	2.06 ± 1.61	2.26 ± 1.12	$P = 0.34$
Exp cross-sectional area, mm^2	2.27 ± 1.65	1.53 ± 0.95	$P < 0.03$
Delta (Exp − Insp), mm^2	0.62 ± 0.86	−0.72 ± 0.59	$P < 0.0002$

Definition of abbreviations: Exp = expiration; Insp = inspiration; NZO = New Zealand Obese; NZW = New Zealand White.

Values are means ± SD. Insp vs. Exp for NZW was significant ($P < 0.006$); Insp vs. Exp for NZO was significant ($P < 0.002$), but in opposite directions.

be false positive, a consideration of all 22 variables taken as a set provides a statistically reliable characterization of NZO versus NZW differences.

Fat in the Pharynx and Neck Region

Analysis of the upper airway images in NZO and NZW mice showed that NZO mice had substantially more subcutaneous and visceral fat in the neck than NZW mice and more fat in the parapharyngeal fat pads (Figures 4 and 5). We quantified these differences (Table 3). The differences in total neck fat and parapharyngeal fat pads volumes between the NZO and NZW mice were highly significant, as was the percentage of fat neck tissue. The volume of fat in the parapharyngeal fat pads in the NZO mice was 3.5 times greater than in the NZW mice.

Size of Upper Airway Structures

There were also differences in the size of upper airway structures between NZO and NZW mice (*see* Table 4, Figures 4 and 5, and Movie E1). Specifically, the NZO mice had significantly increased volumes of the soft palate ($P = 0.021$), tongue ($P = 0.003$) and lateral pharyngeal walls ($P = 0.014$; Table 4) compared with the NZW mice. These findings were not due to general hypertrophy of muscles because the size of the masseter muscles was essentially identical in both mice strains. These data are consistent with the hypothesis that increased fat contributes to increased tongue size among NZO mice when compared with the NZW mice and possibly to increased size of the lateral pharyngeal walls and soft palate. If fat were deposited into all muscles then the masseter muscle would also be larger in the NZO mice than in the NZW mice. These data

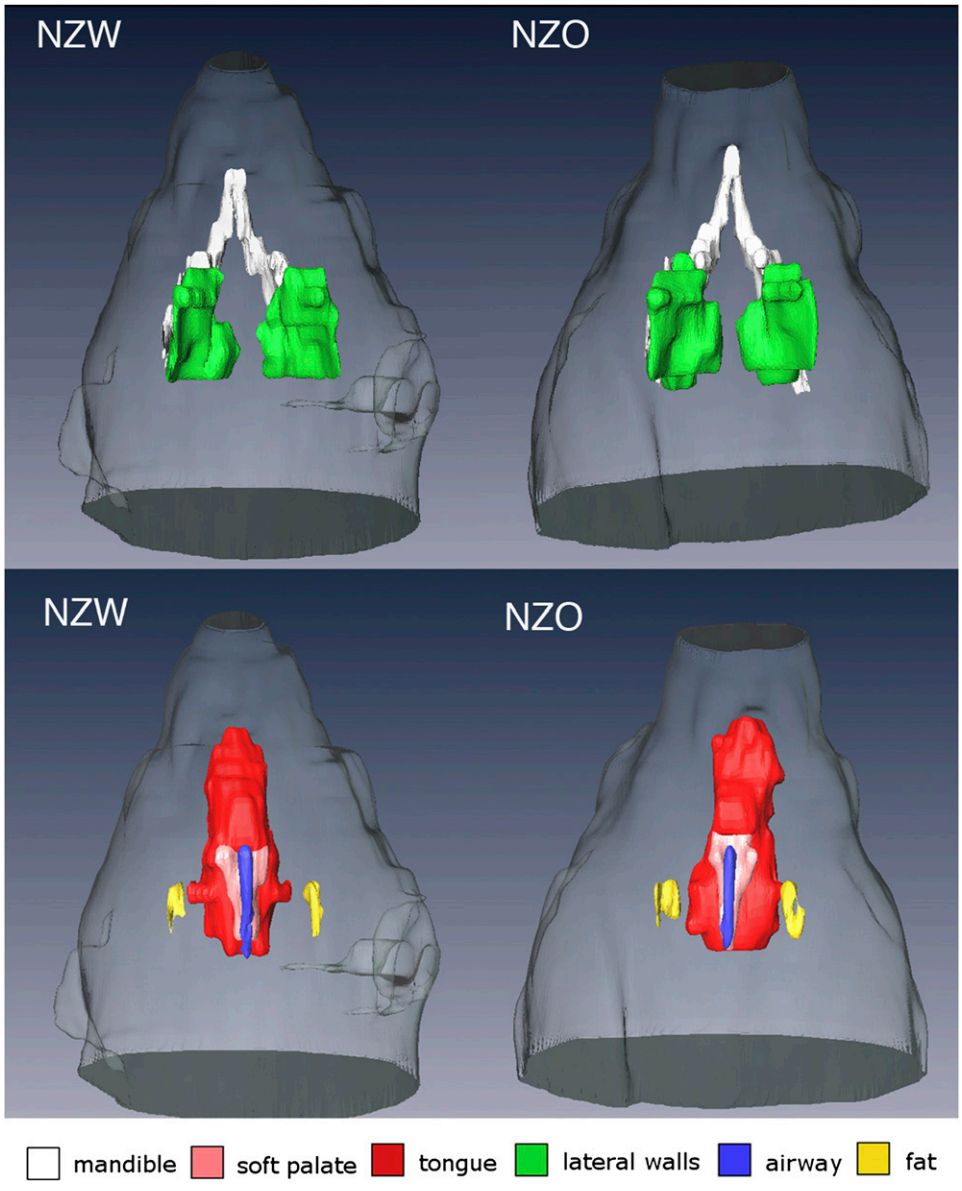

Figure 4. Comparisons of volumetric projection images (dorsal, i.e., brain side) of the upper airway structures in representative New Zealand White (NZW) (*left*) and New Zealand Obese (NZO) (*right*) mice. *Top row* shows the mandible bone (*white*) the width of which is similar in size between the NZW (9.55 mm) and NZO (9.65 mm) mice, but the lateral walls (*green*) are larger in the NZO (120.3 mm^3) compared with the NZW (91.5 mm^3) mice. *Bottom row* is also a dorsal projected view that highlights the tongue: (*red*) (NZW = 126.7 mm^3; NZO = 170.0 mm^3), soft palate (*pink*) (NZW = 4.7 mm^3; NZO = 6.2 mm^3) and parapharyngeal fat pads (*yellow*) (NZW = 1.8 mm^3; NZO = 4.4 mm^3) all of which were larger in volume in NZO mice than in the NZW mice (Tables 2–3) and in these representative mice. Airway volume (*blue*) was slightly smaller in the NZO (1.90 mm^3) compared with the NZW (2.11 mm^3).

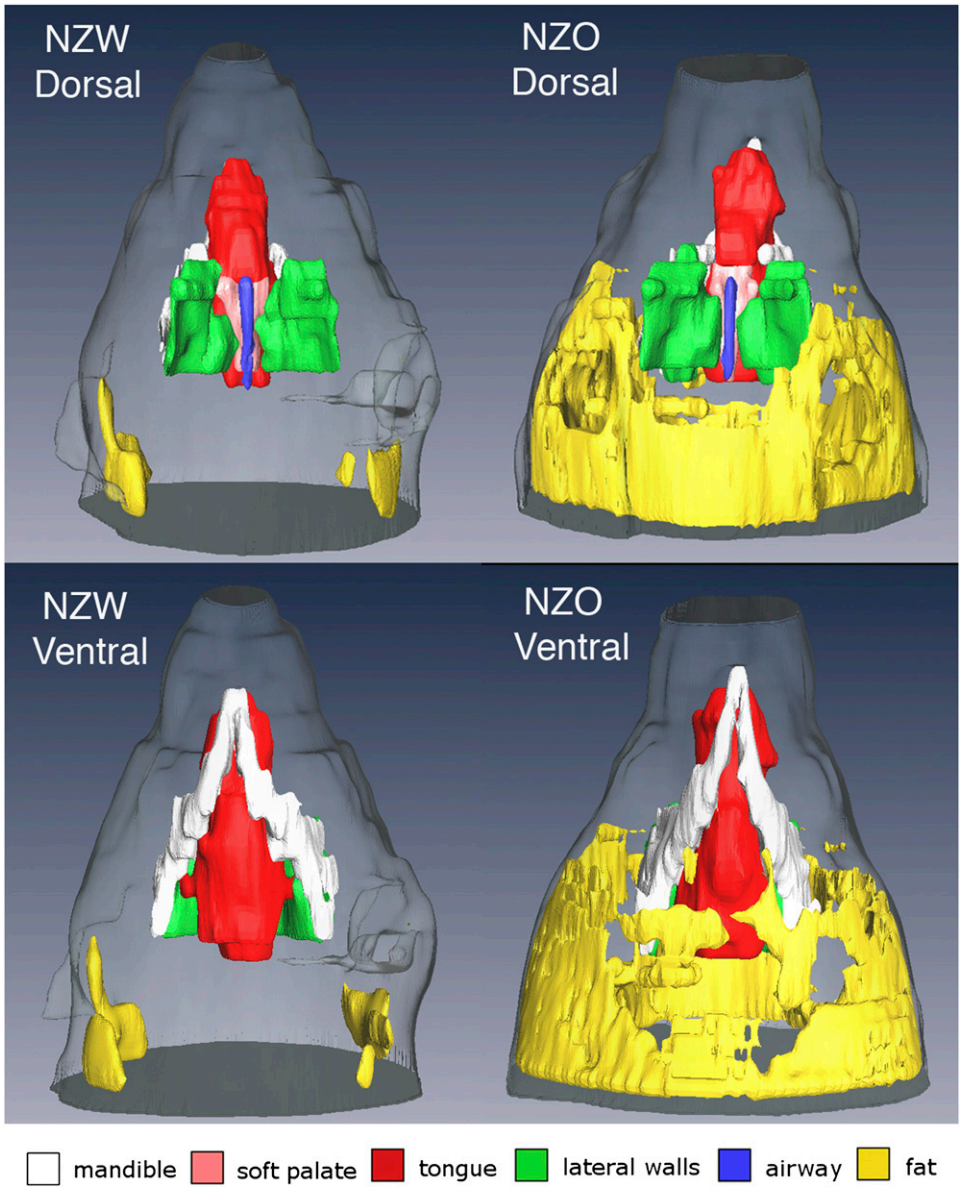

Figure 5. Comparisons of volumetric projection images of the upper airway and neck fat in representative New Zealand White (NZW) (*left*) and New Zealand Obese (NZO) (*right*) mice. *Top row* is the projected view from dorsal side (i.e., brain side); *bottom row* is the projected view from ventral side. In this example, the visceral and subcutaneous fat volume were greater in the NZO (497.0 mm^3) than in the NZW (89.4 mm^3) mouse. Note in the *bottom row* (ventral projection), in the NZO mouse, the fat surrounds the neck including the submental region.

suggest that fat may be selectively deposited in the tongue and other upper airway soft tissue structures, increasing the size of these structures. There was no difference in the width of the mandible (lateral craniofacial measure) or the distance from the upper airway to the back of the head (anterior–posterior craniofacial measure) between the mice strains, indicating that the craniofacial structure between the NZO and NZW mice was similar in size (Table 4).

TABLE 3. FAT IN UPPER AIRWAY REGION

Structures	NZO	NZW	Nominal *P* Value
Total neck fat, mm^3	1940 ± 560	656 ± 390	<0.0001
Neck tissue, mm^3	5470 ± 440	3730 ± 840	0.0001
Neck fat/tissue, %	36 ± 10	17 ± 8	0.0004
Parapharyngeal fat pad volumes, mm^3	5.00 ± 1.37	1.43 ± 0.50	<0.0001

Definition of abbreviations: NZO = New Zealand Obese; NZW = New Zealand White.

Values are means ± SD; n = 12 for NZW; n = 8 for NZO. *P* values were determined using Student's *t* test.

Fat in the Thorax and Abdomen

There was also a substantial increase in fat in the thorax and abdomen (*see* Figures 6 and 7, Table 5, and Movie E2 demonstrating these changes more definitively). In the abdominal region (comparing NZO to NZW in Figure 6), there was an increase in the amount of subcutaneous fat, visceral fat, and fat in the retroperitoneal region around the kidneys (Figure 6, upper abdominal region). The difference in fat amounts between the strains was highly significant in all regions (Table 5). To examine whether the increase was primarily fat related, the ratio of fat to tissue was also compared between the NZO and NZW groups for each region (Table 5). The increase in fat in the NZO mice was not merely a "proportional" increase in both fat and overall tissue because, in all regions (neck thorax, upper and lower abdomen), NZO mice accumulated more fat in proportion to total tissue than the NZW mice. We show in Figure 8 the percentage of increase for different aspects of fat distribution between NZO and NZW mice. These data demonstrate that the differences in amounts between NZO and NZW mice are of similar magnitude in all regions that were assessed.

TABLE 4. SIZE OF PHARYNGEAL STRUCTURES

Structures	NZO	NZW	Nominal *P* Value
Soft palate, mm^3	5.86 ± 1.28	4.64 ± 0.88	0.021
Tongue, mm^3	137 ± 26.0	104 ± 18.0	0.003
Lateral pharyngeal walls, mm^3	111 ± 26.9	84.4 ± 16.2	0.014
Masseter muscle, mm^3	215 ± 33.0	203 ± 31.0	NS ($P = 0.53$)
Mandible width, mm	7.85 ± 0.37	7.9 ± 0.34	NS ($P = 0.76$)
A–P distance, mm	5.46 ± 0.34	5.2 ± 0.22	NS ($P = 0.501$)

Definition of abbreviations: A–P = anterior to posterior distance from airway to back of head; NS = not significant; NZO = New Zealand Obese; NZW = New Zealand White.

Values are means ± SD; n = 12 for NZW; n = 8 for NZO. *P* values were determined using Student's *t* test.

DISCUSSION

Obesity is the most important risk factor for OSA (1–3). Obese subjects with OSA have a narrowed upper airway during wakefulness and an enlargement of the upper airway structures (4–8). Why obesity leads to altered upper airway structure and upper airway compromise is currently unknown. Investigation of obese animal models, in particular mice, provides a novel approach to study this relationship. There are multiple models of obesity in mice that are available for study (37, 38). Moreover, regional distribution of fat in rodents (39) and humans (15, 40) is under strong genetic control.

Volumetric MRI has been shown to be a powerful modality to examine the upper airway in humans and to distinguish anatomic differences between subjects with apnea and normal controls (6). We used volumetric MRI in obese NZO mice and lean NZW mice in this study to examine upper airway size and the surrounding structures as well as visceral fat. We have shown that the obese NZO mouse has much more visceral fat in all regions than the NZW mouse. It has more neck fat, including a substantial increase in the volume of the parapharyngeal fat pads. We have also demonstrated that the volume of the tongue, soft palate, and lateral pharyngeal walls are larger in the NZO mouse than in the NZW mouse, as they are in humans with OSA (6). We propose that this is a result of fat infiltrating these structures. The enlargement of these upper airway soft tissue structures is associated with altered physiology of the upper airway of the NZO mouse. This is the first time that regional visceral fat and the upper airway structures have been quantified in three dimensions using MRI with a mouse model. The NZO mouse has altered anatomical features in the upper airway and surrounding soft tissues that are analogous to those described in humans with OSA (6, 27, 30, 41).

Study Design and Methodology

We used magnetic resonance upper airway imaging paradigms and analysis strategies to study the NZO and NZW mouse. The MRI protocol was optimized to achieve specific goals for high-resolution thin slice (1.0 mm) gated imaging in the head and

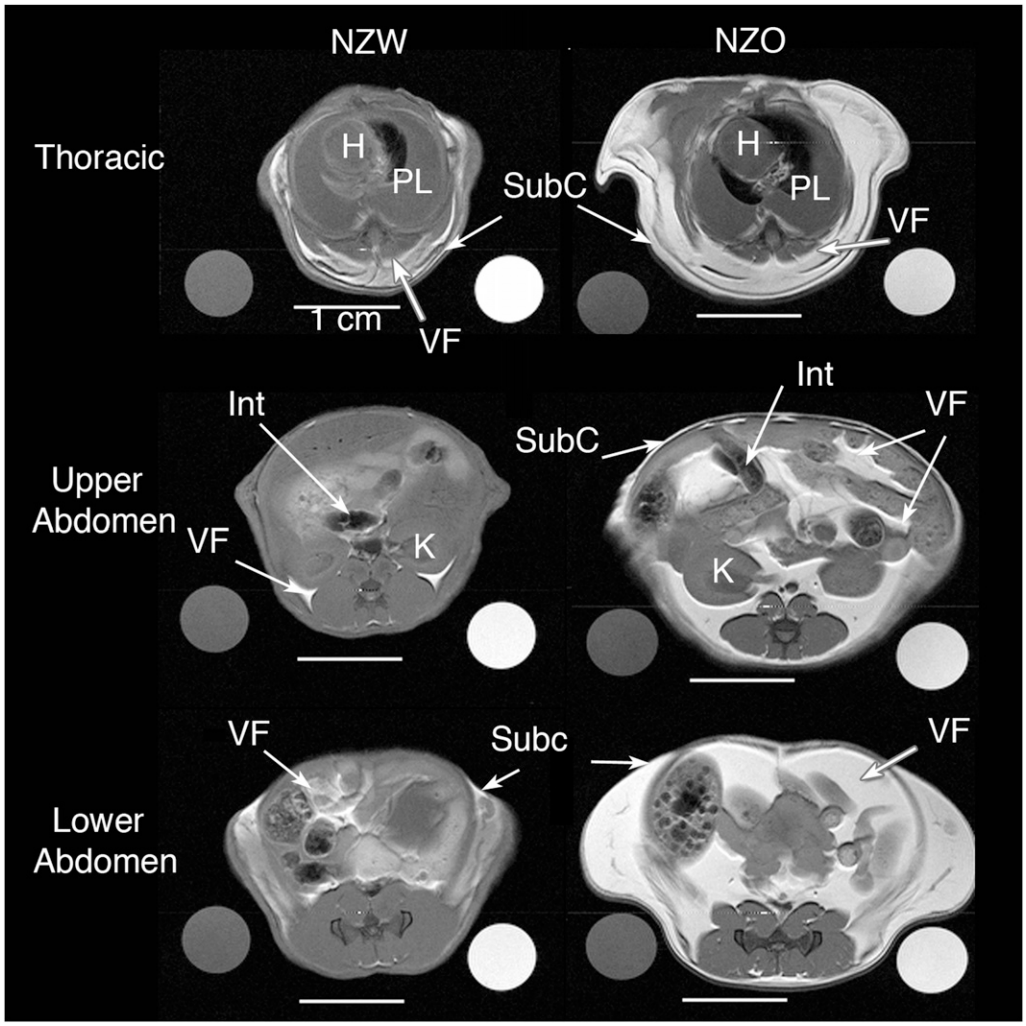

Figure 6. Axial magnetic resonance image of New Zealand White (NZW) (*left side*) and New Zealand Obese (NZO) (*right side*) showing comparisons of visceral and subcutaneous fat in the thoracic region (*top row*), upper abdominal region (*middle row*) and lower abdominal region (*bottom row*). The axial spin-echo proton weighted images show soft tissue contrast and fat content. On the sides of each of the six image panels there are circular cross-sections of the water (*left*) and oil phantoms (*right*). The 2-mm thick axial images are representative of NZW and NZO mice. In all cases there is more visceral fat and subcutaneous fat in the NZO than in the NZW mice. H = heart; PL = pleural space (partially filled with fluid, as these images were acquired in postmortem mice following KCl intracardiac injection for euthanasia); SubC = subcutaneous fat; VF = visceral fat; Int = intestines; K = kidney.

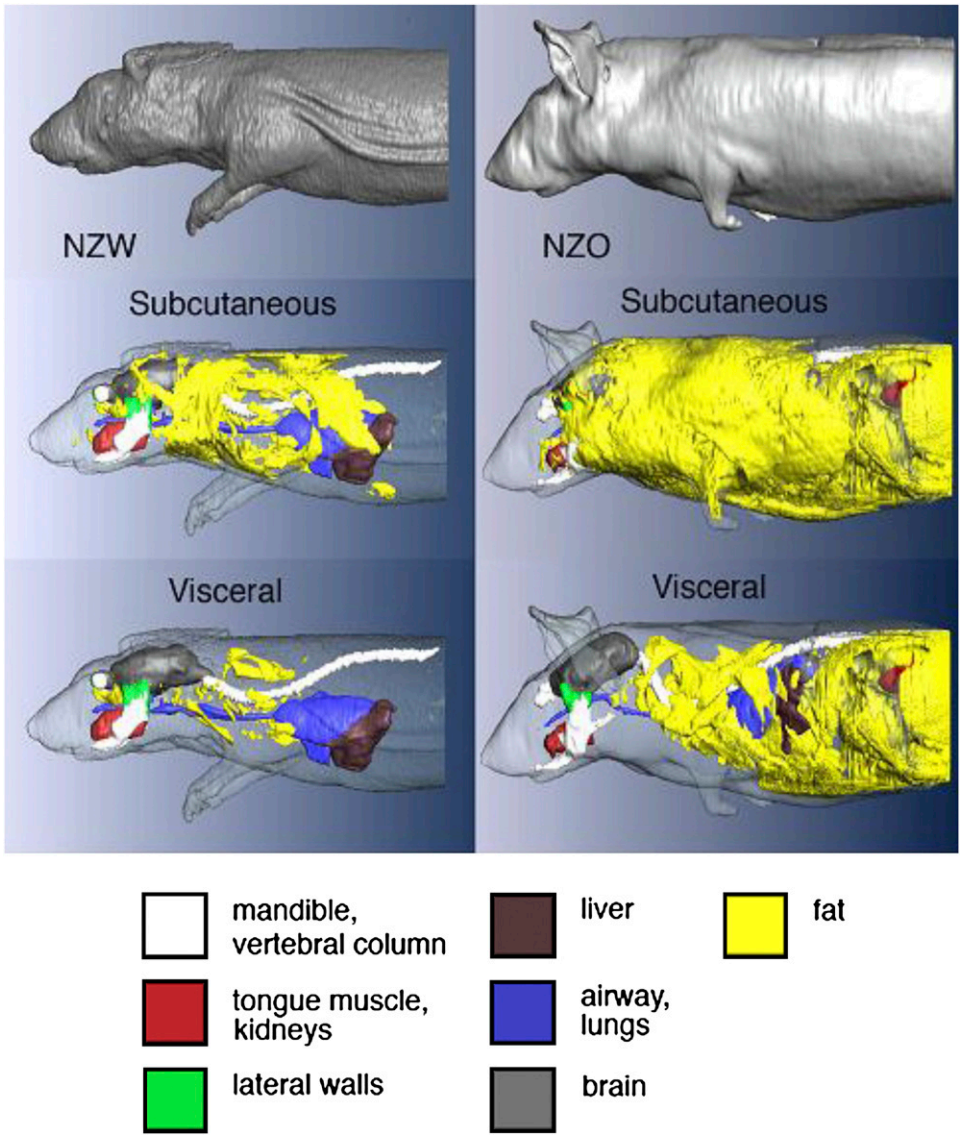

Figure 7. 3D volume renderings of New Zealand White (NZW) (*left*) and New Zealand Obese (NZO) (*right*) mice from the head to the region of the lower abdomen. *Top row* shows surface boundary of the mouse body, *middle row* shows subcutaneous fat layers, and *bottom row* shows cutaway highlighting visceral fat and organs (subcutaneous fat and body surface are rendered translucent). There is substantially more subcutaneous and visceral fat in the NZO mouse than in the NZW mouse. MRI was obtained using a 3D spin-echo protocol with isotropic voxel size = 0.156 mm.

pharynx where structures are small. The respiratory-gated protocol we used substantially eliminated the respiratory-related motion artifact and allowed an *in-vivo* assessment of airway size in expiration. Whole-body imaging was performed using thicker slices (2.0 mm), which resulted in greater signal-to-noise ratios, and our use of studies in the post-mortem mouse eliminated long imaging time under anesthesia. This allowed very precise assessment of regional fat distribution.

Although imaging was performed differently for the upper airway and body of the mice, these MRI methods represent a significant advancement over other methods that have been used to obtain phenotypic information about fat distribution and upper airway anatomy in the mouse. Previous studies in rodents have used physical methods, such as whole-body and regional dissection and analysis of fat deposits (42–44), or histological (microscopic) analysis of tissues (45). Whereas chemical analysis and dissection methods have been used for determining fat content in rodents, recent studies indicate that quantitative MRI provides more reliable measurements of fat content in rats and mice (43, 46). Particularly in smaller animals, where dissection cannot easily separate organs and regional boundaries, noninvasive MRI techniques for measuring fat volume and distribution are preferable (46). They provide detailed anatomical information in addition to fat distribution maps (45). They also allow *in-vivo* measurements, thereby permitting longitudinal studies in the same animals, and provide for physiologic conditions during the image acquisition (47).

Although this is not the first study on obese mice using MRI techniques (48, 49), we combined a detailed MRI of the upper airway structures with whole-body volumetric analysis for fat discrimination (Dixon protocol) together with gradient-echo respiratory dynamic imaging to provide an anatomic and functional examination of the NZW and NZO mice. The advantage of our imaging protocol involves use of the Dixon 3 point method for fat/water discrimination (32). The Dixon method is a spin echo spectroscopic imaging technique that uses the chemical shift difference between hydrogen protons bounded in water (H_2O) and lipids (CH_3) to generate two separate images (50). In our study, the Dixon fat–weighted images were used to assess the fat volume in axial slices using a thresholding method, whereby a white signal intensity over a given threshold in the image pixels was counted as fat. A mineral oil phantom was included in all axial slices so that the image intensity of that lipid source was used as the lower threshold in the fat-weighted images. In this way interslice and interanimal variations in fat-weighted image intensity were normalized. We adapted methods from Zhang and

TABLE 5. REGIONAL FAT DISTRIBUTION (VOLUMES)

Tissue Type	NZO	NZW	Nominal *P* Value
Thoracic			
Fat, mm^3	4260 ± 850	1290 ± 520	<0.0001
Tissue, mm^3	8440 ± 140	575 ± 101	0.0002
Fat/tissue, %	50 ± 3	20 ± 9	<0.0001
Upper Abdomen			
Subcutaneous fat, mm^3	1250 ± 530	426 ± 270	0.0005
Visceral fat, mm^3	3570 ± 752	1010 ± 480	<0.0001
Tissue, mm^3	11700 ± 3470	8300 ± 2100	0.0031
Fat/tissue, %	43 ± 9	21 ± 12	0.0005
Lower Abdomen			
Subcutaneous fat, mm^3	4230 ± 840	1960 ± 990	0.0001
Visceral fat, mm^3	3550 ± 840	1700 ± 790	0.0002
Tissue, mm^3	13400 ± 2200	9730 ± 1790	0.0006
Fat/tissue, %	58 ± 4	37 ± 16	0.0031

Definition of abbreviations: See Table 3.
Values are means ± SD. *P* values were determined using Student's *t* test.

colleagues (45), who evaluated liver fat in rats using oil and water phantoms for in-plane image calibration of fat-weighted intensity. They provided a validation of the quantitative Dixon-method MRI by comparing the Dixon liver fat measurements with histological and chemical analysis of fat infiltration in rat livers (45).

Upper Airway Compromise in NZO Mice

Both the NZO and NZW mice maintain patency throughout the respiratory cycle. We compared airway dimensions in the hypopharyngeal region between genotypes because the airway at this level is surrounded by muscle and soft tissue, and the airway in the mouse at this point distal to the caudal edge of the soft palate is comprised of a single lumen. The NZO mouse has a smaller airway cross-sectional area than the NZW mouse in expiration. We also found at the hypopharyngeal level that the pharyngeal airway caliber of the NZW mouse is larger during expiration than during inspiration. The NZW respiratory pattern is similar to the within-breath changes in upper airway dimensions found in normal humans (51, 52). This respiratory pattern is likely related to the upper airway being relatively passive in normal subjects with the expiratory widening of the airway being due to the positive intraluminal pressure during expiration. The inspiratory and expiratory difference in airway dimensions in the NZO is opposite to that in the NZW. The airway of the NZO is larger in inspiration than expiration. The NZO pattern (inspiratory cross-sectional area was increased in inspiration compared with expiration) is an unusual pattern that suggests increased motor activation of the upper airway dilator muscles during inspiration. This pattern has been observed in the awake English bulldog, who also exhibits apneas, particularly during REM sleep (24). The respiratory patterns of the English bulldog and NZO mouse are compatible with the concept that these animals have, as a consequence of upper airway compromise, increased inspiratory upper airway motor activation to overcome the negative intraluminal pressures during inspiration. In the English bulldog, there is marked activation of upper airway muscles during inspiration as revealed by electromyograms (24).

Although the present investigation does not prove directly the reason for upper airway narrowing in the NZO mouse, it seems most likely that this is due to the increased size of the upper airway soft tissue structures that we found within the bounds of the same craniofacial structure as the lean NZW. There are, however, alternative possibilities. The obesity of the NZO mouse could produce a mass loading effect on the thorax, thus reducing functional residual capacity. In humans, reductions in functional residual capacity result in narrowing of the upper airway due to reduction in tracheal tug on the upper airway (53). We did not measure functional residual capacity in our studies, although this measurement can be obtained noninvasively using sophisticated micro-CT methods (54) or complex plethysmography (55). As Tankersley and colleagues have shown (56), differences in lung mechanics are found in different mouse strains. Thus, we cannot exclude the possibility that upper airway changes in the obese NZO mouse are at least partially due to reduced functional residual capacity. Another possibility, that we believe is unlikely, is that the neck positions in the NZO and NZW mice were different, with the NZO having a more flexed posture. We believe this is unlikely because a fixed apparatus was used to hold mice during imaging, and we have shown (in a representative group of both NZW and NZO mice) that the head-to-neck angle was not significantly different in NZO and NZW mice during the MRI studies.

Size of Upper Airway Soft Tissue Structures in the NZO Mouse

A central hypothesis of this investigation was that the size of the upper airway soft tissue structures was larger in the NZO mice than in the NZW mice. Our data support this hypothesis. We found increased volume of the tongue, lateral pharyngeal walls, and soft palate in the NZO mice when compared with the NZW mice. There were no differences in the width of the mandible between the NZO and NZW mice. Thus, the smaller airway caliber in NZO mice is likely the result of the enlargement in the volume of the soft-tissue structures within the confines of the same size craniofacial structure (7, 57).

These data raise the question as to why the upper airway soft tissue structures are enlarged in the NZO mice. In humans, the size of these upper airway structures soft tissue structures are heritable (58) so that genetic factors are likely playing a role in the enlargement of these structures. Genes associated with

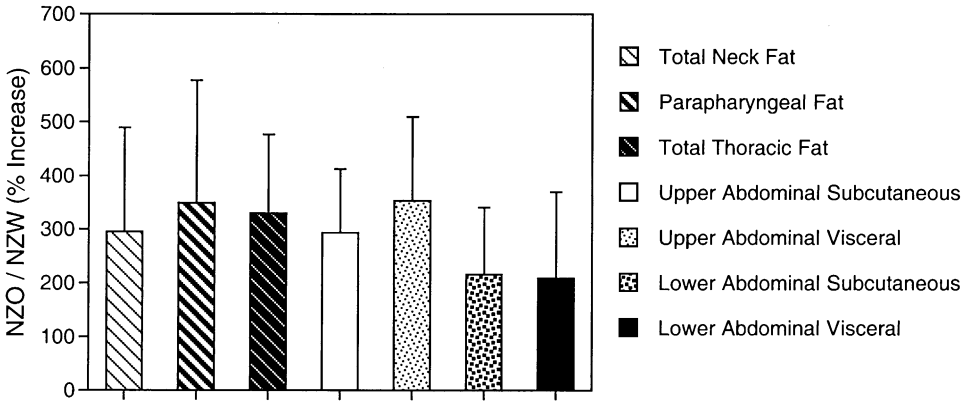

Figure 8. Bar graph demonstrating increased percentage of fat in New Zealand Obese (NZO) compared with New Zealand White (NZW) by region. Increased fat is found in all regions of the NZO mouse. The large increase in fat in the NZO and NZW mice did not differ significantly between the regions studied and between subcutaneous and visceral compartments. Error bars show the SD of the ratio of the mean calculated by standard error analysis (65).

muscle development (for the muscular structures—tongue and lateral pharyngeal walls) may play an important role in determining the size of these structures (58). There are a number of plausible candidate genes (for example, muscle-specific genes coding for proteins, such as desmin, myosin, actin, troponin, and tropomysin; genes for muscle creatine kinase and the Myogenic Regulatory Factors) (59–62) that could explain enlargement of the upper airway soft tissue structures.

However, our data also suggest another possibility. Tongue enlargement in NZO mice may be directly due to fat deposition. The tongue is composed of muscular and fatty tissue. An autopsy study (26) demonstrated that the human tongue has a remarkably high percentage of fat and that increasing tongue weight and percentage of tongue fat are associated with increasing obesity. Apnea was not examined in that study. These data argue that tongue fat is likely to be important in understanding the relationship between obesity and narrowing of the upper airway. Our study was not designed to investigate tongue fat. However, we were able to perform a histologic analysis of the tongue in a preliminary study of one NZO mouse and one NZW mouse (Figure 9). Figure 9 shows 40-μm sections from NZO and NZW mice stained with hematoxylin-eosin to highlight fat (white) in the tongue muscle tissue. There is much more fat in the tongue of an NZO mouse than in the tongue of a NZW mouse. (The insert on Figure 9 shows higher pair image [×40] of tongue tissue taken from the center of both tongues that indicates the increased fat between muscle fibers from the NZO sample versus the NZW sample).

Fat Distribution in the NZO Mouse

NZO mice had a large increase in the volume of the parapharyngeal fat pads. These fat deposits have been thought to play a particularly important role in humans in the pathogenesis of OSA (6, 7, 25, 57). Even in nonobese human subjects with OSA, the volume of these fat pads is increased compared with weight-matched controls (25). Thus, there may be particular genetic influences on this aspect of fat distribution with particular relevance to the effects of obesity on the upper airway. The NZO mouse not only has increased fat in the parapharyngeal fat pads but also has significant increases in fat in the neck, thorax, and abdomen (Tables 3 and 5). This increase was found in both the subcutaneous and visceral compartments. The percentage of increase in fat in these different compartments and regions between NZO and lean NZW mice was similar and did not differ significantly between regions. We know from human studies that visceral fat in particular is associated with the metabolic syndrome (63) and cardiovascular disease (64).

In this study we showed that obesity narrows the static and dynamic upper airway of obese mice. We have shown that obese mice have enlarged tongues and deposit fat into their tongues. Our results provide a paradigm for future studies to examine differences in obese and nonobese mice using other physiologic measurements including (*1*) electromyogram activity of the upper airway muscles, (*2*) sleep architecture, and (*3*) critical collapsing pressure (Pcrit). Such studies would provide data on the effect of obesity on each of these physiologic measurements.

CONCLUSION

In conclusion, we used volumetric MRI to show that the size of upper airway soft tissue structures and the volume of visceral fat is greater in the NZO mouse than in the NZW mouse. In particular, the size of the tongue, lateral pharyngeal walls, soft palate, and parapharyngeal fat pads were greater in the NZO mice when compared with NZW mice. We showed that obese mice have enlarged tongues and deposit fat directly in the tongue. Upper airway size is diminished in the NZO mouse compared with the NZW mouse. Moreover, the NZO mice demonstrated inspiratory phasic dilation of the pharynx (i.e., upper airway caliber was larger in inspiration than expiration, in direct contrast to the NZW, where upper airway caliber was reduced during inspiration). The experimental approach we used in this study opens a new line of investigation into effects of obesity in mice because we combined physiological features (dynamic respiratory imaging) with noninvasive MRI that so that evaluations could be performed on a functional and anatomic basis. Importantly, our data support a novel hypothesis to explain why obesity is strongly associated with OSA (i.e., direct fat deposits in the tongue that enlarge tongue size as well as

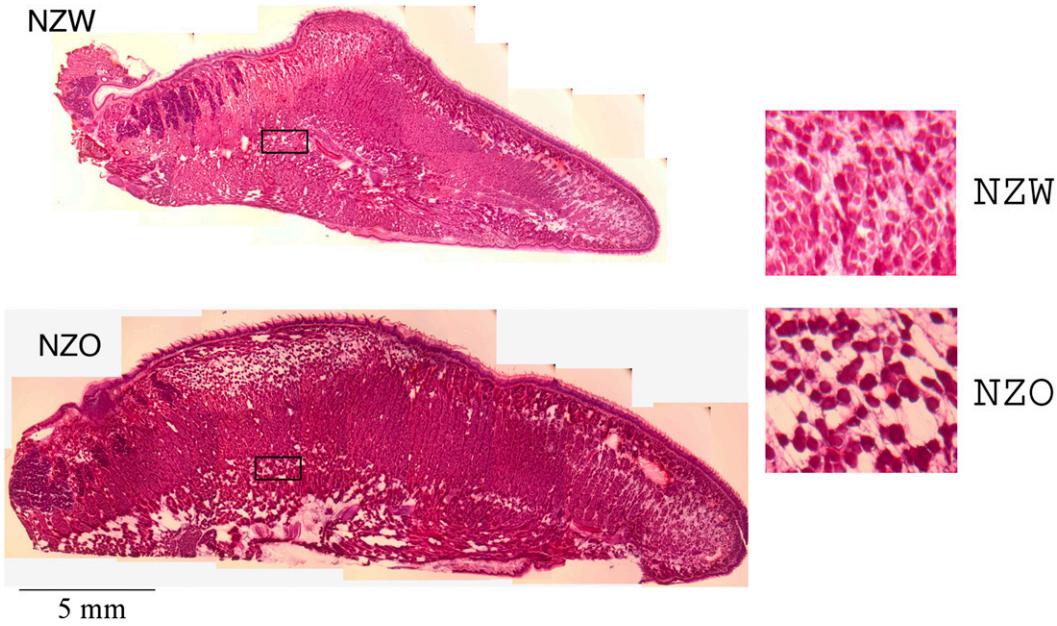

Figure 9. Histological comparison of fat in the tongues of New Zealand White (NZW) and New Zealand Obese (NZO) mice. Mid-sagittal slices (40 μm; mouse weights: NZW = 322 gm, NZO = 680 gm) sections were prepared from freshly frozen tissue and stained with HandE. Fat is unstained (*white*); muscle is stained (*red*). The mid-sagittal image shows substantially more tongue fat in multiple tongue regions in the NZO mouse than in the NZW mouse. *Inset*: Comparison of tissue at matched mid-transverse locations (boxed outline in each tongue) at high magnification (×40). The muscle fibers are stained red, with fat being clear. There is more fat deposited between muscle fibers of the tongue from NZO mice compared with that from NZW mice.

other upper airway structures) thereby leading to a smaller upper airway as occurs in patients with OSA.

Conflict of Interest Statement: None of the authors has a financial relationship with a commercial entity that has an interest in the subject of this manuscript.

Acknowledgments: The authors acknowledge the technical expertise of Kathy Zhang, Sarika Shinde and Raymond Galante in conduct of these studies and the support staff of the Small Animal Imaging Facility, Department of Radiology, University of Pennsylvania. We are grateful to our colleagues at the Jackson Laboratory (Bar Harbor, Maine), Dr. Bev Paigen, Dr. Luanne Peters, and Ms. Karen Svenson, for bringing the NZO mouse to our attention and for providing the pictures (Figure E1) in the online supplement. We acknowledge the help of Daniel Barrett in preparation of this manuscript.

References

1. Strobel RJ, Rosen RC. Obesity and weight loss in obstructive sleep apnea: a critical review. *Sleep* 1996;19:104–115.
2. Fogel RB, Malhotra A, Dalagiorgou G, Robinson MK, Jakab M, Kikinis R, Pittman SD, White DP. Anatomic and physiologic predictors of apnea severity in morbidly obese subjects. *Sleep* 2002;26:150–155.
3. Dixon JB, Schachter LM, O'Brien PE. Polysomnography before and after weight loss in obese patients with severe sleep apnea. *Int J Obes* 2005;29:1048–1054.
4. Horner RL, Mohiaddin RH, Lowell DG, Shea SA, Burman ED, Longmore DB, Guz A. Sites and sizes of fat deposits around the pharynx in obese patients with obstructive sleep apnea and weight matched controls. *Eur Respir J* 1989;2:613–622.
5. Ryan CF, Love LL. Mechanical properties of the velopharynx in obese patients with obstructive sleep apnea. *Am J Respir Crit Care Med* 1996;154:806–812.
6. Schwab RJ, Pairstein M, Pierson R, Mackley A, Hachadoorian R, Arens R, Maislin G, Pack AI. Identification of upper airway anatomic risk factors for obstructive sleep apnea with volumetric magnetic resonance imaging. *Am J Respir Crit Care Med* 2003;168:522–530.
7. Shelton KE, Woodson H, Gay SB, Suratt PM. Pharyngeal fat in obstructive sleep apnea. *Am Rev Respir Dis* 1993;148:462–466.
8. Haponik EF, Smith PL, Bohlman ME, Allen RP, Goldman SM, Bleecker ER. Computerized tomography in obstructive sleep apnea. *Am Rev Respir Dis* 1983;127:221–226.
9. Brennick MJ, Pickup S, Cater JC, Kuna ST. Phasic respiratory pharyngeal mechanics by magnetic resonance imaging in lean and obese Zucker rats. *Am J Respir Crit Care Med* 2006;173:1031–1037.
10. Magalang UJ, Farkas GA, Najdzionek JS, Nakano H. Obese Zucker rats have narrower upper airway compared to lean litter-mates. *Am J Respir Crit Care Med* 2000;161:A87. (abstract).
11. Magalang UJ, Ray AD, Farkas GA. Effects of hypoglossal nerve stimulation on upper airway mechanics in obese Zucker rats. *Am J Respir Crit Care Med* 2002;165:A798.
12. Nakano H, Magalang UJ, Lee S-d, Krasney JA, Farkas GA. Serotonergic modulation of ventilation and upper airway stability in obese Zucker rats. *Am J Respir Crit Care Med* 2001;163:1191–1197.
13. Lonergan RP III, Ware JC, Atkinson RL, Winter WC, Suratt PM. Sleep apnea in obese miniature pigs. *J Appl Physiol* 1998;84:531–536.
14. Tuck SA, Dort JC, Olson ME, Remmers JE. Monitoring respiratory function and sleep in the obese Vietnamese pot-bellied pig. *J Appl Physiol* 1999;87:444–451.
15. Bouchard C. Genetic determinants of regional fat distribution. *Hum Reprod* 1997;12:1–5.
16. Brockmana GA, Bevova MR. Using mouse models to dissect the genetics of obesity. *Trends Genet* 2002;18:367–376.
17. Chen Y, Rollins J, Paigen B, Wang X. Genetic and genomic insights into the molecular basis of atherosclerosis. *Cell Metab* 2007;6:164–179.
18. Peters LL, Robledo RF, Bult CJ, Churchill GA, Paigen BJ, Svenson KL. The mouse as a model for human biology: a resource guide for complex trait analysis. *Nat Rev Genet* 2007;8:58–69.
19. Taylor BA, Wnek C, Schroeder D, Phillips SJ. Multiple obesity QTLs identified in an intercross between the NZO (New Zealand obese) and the SM (small) mouse strains. *Mamm Genome* 2001;12:95–103.
20. Bielschowsky M, Goodall CM. Origin of inbred NZ mouse strains. *Cancer Res* 1970;30:834–836.
21. Vernoi MC, Proietto J, Larkins RG. Evolution of insulin resistance in New Zealand obese mice. *Diabetes* 1991;40:1480–1487.
22. Ortlepp JR, Kluge R, Giesen K, Plum L, Radke P, Hanrath P, Joost H-G. A metabolic syndrome of hypertension, hyperinsulinaemia and hypercholesterolaemia in the New Zealand obese mouse. *Eur J Clin Invest* 2000;30:195–202.
23. Igel M, Becker W, Herberg L, Joost H-G. Hyperleptinemia, leptin resistance, and polymorphic leptin receptor in the New Zealand obese mouse. *Endocrinology* 1997;138:4234–4239.
24. Veasey SC, Panckeri KA, Hoffman EA, Pack AI, Hendricks JC. The effects of serotonin antagonists in an animal model of sleep disordered breathing. *Am Rev Respir Dis* 1996;153:776–786.
25. Mortimore IL, Marshall I, Wraith PK, Sellar RJ, Douglas NJ. Neck and total body fat deposition in nonobese and obese patients with sleep apnea compared with that in control subjects. *Am J Respir Crit Care Med* 1998;157:280–283.
26. Nashi N, Kang S, Barkdull GC, Lucas J, Davidson TM. Lingual fat at autopsy. *Laryngoscope* 2007;117:1467–1473.
27. Schwab RJ, Pairstein M, Kaplan L, Pierson R, Mackley A, Hachadoorian R, Arens R, Maislin G, Pack AI. Family aggregation of upper airway soft tissue structures in normal subjects and patients with sleep apnea. *Am J Respir Crit Care Med* 2006;173:453–463.
28. Zohar Y, Sabo R, Strauss M, Schwartz A, Gal R, Oksenberg A. Oropharyngeal fatty infiltration in obstructive sleep apnea patients: a histologic study. *Ann Otol Rhinol Laryngol* 1998;107:170–174.
29. Boyd JH, Petrof BJ, Hamid Q, Fraser R, Kimoff RJ. Upper airway muscle inflammation and denervation changes in obstructive sleep apnea. *Am J Respir Crit Care Med* 2004;170:541–546.
30. Schwab RJ, Gupta KB, Gefter WB, Metzger LJ, Hoffman EA, Pack AI. Upper airway and soft tissue anatomy in normal subjects and patients with sleep disordered breathing. *Am J Respir Crit Care Med* 1995;152:1673–1689.
31. Hendricks JC, Kline LR, Kovalski RJ, O'Brien JA, Morrison AR, Pack AI. The English bulldog: a natural model of sleep-disordered breathing. *J Appl Physiol* 1997;63:1344–1350.
32. Glover GH, Schneider E. Three-point Dixon technique for true water/fat decomposition with b inhomogeneity correction. *Magn Reson Med* 1991;18:371–383.
33. Ko K, Pack A, Schwab R, Pickup S, Zhang K, Chmielewski L, Peters LL, Svenson KL, Paigen BJ, Galante R, *et al.* MRI of NZO and NZW mice, identification of a mouse strain with a compromised upper airway and increased parapharyngeal fat. *Proc Am Thorac Soc* 2006;3:A315.
34. Benjamini Y, Hochberg Y. Controlling the false discovery rate: a practical and powerful approach to multiple testing. *J R Statist Soc B* 1995;57:289–300.
35. Sabatti C, Service S, Freimer N. False discovery rate in linkage and association genome screens for complex disorders. *Genetics* 2003;164:829–833.
36. Nichols T, Hayasaka S. Controlling the familywise error rate in functional neuroimaging: a comparative review. *Stat Methods Med Res* 2003;12:419–446.
37. Lindstrom P. The physiology of obese-hyperglycemic mice (ob/ob mice). *ScientificWorldJournal* 2007;7:666–685.
38. Pomp D, Nehrenberg D, Estrada-Smith D. Complex genetics of obesity in mouse models. *Annu Rev Nutr* 2008;28:331–345.
39. Stylianou IM, Korstanje R, Li R, Sheehan S, Paigen B, Churchill GA. Quantitative trait locus analysis for obesity reveals multiple networks of interacting loci. *Mamm Genome* 2006;17:22–36.
40. Borecki IB, Rice T, Perusse L, Bouchard C, Rao DC. Major gene influence on the propensity to store fat in trunk versus extremity depots: evidence from the Quebec Family Study. *Obes Res* 1995;3:1–8.
41. Horner RL, Shea SA, McIvor J, Guz A. Pharyngeal size and shape during wakefulness and sleep in patients with obstructive sleep apnea. *Q J Med New Series* 1989;72:719–735.
42. Ross R, Leger L, Guardo R, Guise JD, Pike BG. Adipose tissue volume measured by magnetic resonance imaging and computerized tomography in rats. *J Appl Physiol* 1991;70:2164–2172.
43. Tang H, Vasselli JR, Wu EX, Boozer CN, Gallagher D. High-resolution magnetic resonance imaging tracks changes in organ and tissue mass in obese and aging rats. *Am J Physiol Regul Integr Comp Physiol* 2002;282:R890–R899.
44. Hausman DB, Fine JB, Tagra K, Fleming SS, Martin RJ, DiGirolamo M. Regional fat pad growth and cellularity in obese Zucker rats: modulation by caloric restriction. *Obes Res* 2003;11:674–682.
45. Zhang X, Tengowski M, Fasulo L, Botts S, Suddarth SA, Johnson GA. Measurement of fat/water ratios in rat liver using 3D three-point Dixon MRI. *Magn Reson Med* 2004;51:697–702.
46. Taicher GZ, Tinsley FC, Reiderman A, Heiman ML. Quantitative magnetic resonance (QMR) method for bone and whole-body-composition analysis. *Anal Bioanal Chem* 2003;377:990–1002.
47. Zhou R, Pickup S, Glickson JD, Scott CH, Ferrari VA. Assessment of global and regional myocardial function in the mouse using cine and tagged MRI. *Magn Reson Med* 2003;49:760–764.

48. Calderan L, Marzola P, Nicolato W, Fabene PF, Milanese C, Bernardi P, Giordano A, Cinti S, Sbarbati A. In vivo phenotyping of the ob/ob mouse by magnetic resonance imaging and ^{1}H-magnetic resonance spectroscopy. *Obesity (Silver Spring)* 2006;14:405–414.
49. Walling BE, Munasinghe J, Berrigan D, Bailey MQ, Simpson RM. Intra-abdominal fat burden discriminated in vivo using proton magnetic resonance spectroscopy. *Obesity (Silver Spring)* 2007;15:69–77.
50. Dixon WT. Simple proton spectroscopic imaging. *Radiology* 1984;153: 189–194.
51. Schwab RJ, Gefter WB, Hoffman EA, Gupta KB, Pack AI. Dynamic upper airway imaging during awake respiration in normal subjects and patients with sleep disordered breathing. *Am J Respir Crit Care Med* 1993;148:1385–1400.
52. Schwab RJ, Gefter WB, Pack AI, Hoffman EA. Dynamic imaging of the upper airway during respiration in normal subjects. *J Appl Physiol* 1993;74:1504–1514.
53. Tagaito Y, Isono S, Remmers JE, Tanaka A, Nishino T. Lung volume and collapsibility of the passive pharynx in patients with sleep-disordered breathing. *J Appl Physiol* 2007;103:1379–1385.
54. Mitzner W, Brown R, Lee W. In vivo measurement of lung volumes in mice. *Physiol Genomics* 2001;4:215–221.
55. Janosi TZ, Adamicza A, Zosky GR, Asztalos T, Sly PD, Hantos Z. Plethysmographic estimation of thoracic gas volume in apneic mice. *J Appl Physiol* 2006;101:454–459.
56. Tankersley CG, Rabold R, Mitzner W. Differential lung mechanics are genetically determined in inbred murine strains. *J Appl Physiol* 1999; 86:1764–1769.
57. Shelton KE, Gay SB, Hollowell DE, Woodson H, Suratt PM. Mandible enclosure of upper airway and weight in obstructive sleep apnea. *Am Rev Respir Dis* 1993;148:195–200.
58. Schwab RJ. Genetic determinants of upper airway structure. *Respir Physiolo Neurobiol* 2005;147:289–298.
59. Darlymple KR, Prigozy TI, Mayo M, Kedes L, Shuler CF. Murine tongue muscle displays a distinct developmental profile of MRF and contractile gene expression. *Int J Dev Biol* 1999;43:27–37.
60. Ludolph DC, Konieczny SF. Transcription factor families: muscling in on the myogenic program. *FASEB J* 1995;9:1595–1604.
61. Nguyen QG, Buskin JN, Himeda CL, Shield MA, Hauschka SD. Differences in the function of three conserved E-boxes of the muscle creatine kinase gene in cultured myocytes and in transgenic mouse skeltal and cardiac muscle. *J Biol Chem* 2003;278:46494–46505.
62. Shuler CF, Darlymple KR. Molecular regulation of tongue and craniofacial muscle differentiation. *Crit Rev Oral Biol Med* 2001;12:3–17.
63. Fox CS, Massaro JM, Hoffmann U, Pou KM, Maurovich-Horvat P, Liu CY, Vasan RS, Murabito JM, Meigs JB, Cupples LA, *et al.* Abdominal visceral and subcutaneous adipose tissue compartments: association with metabolic risk factors in the Framingham Heart Study. *Circulation* 2007;116:39–48.
64. Matsuzawa Y, Shimomura I, Nakamura T, Keno Y, Tokunaga K. Pathophysiology and pathogenesis of visceral fat obesity. *Ann N Y Acad Sci* 1993;676:270–278.
65. Taylor JR. An introduction to error analysis: the study of uncertainties in physical measurements, Series of books in physics. Mill Valley, CA: University Science Books, 1982.